*American Mineralogist, Volume 74, pages 1233–1246, 1989*

# Mineralogy in two dimensions: Scanning tunneling microscopy of semiconducting minerals with implications for geochemical reactivity

**Michael F. Hochella, Jr.**
Department of Geology, Stanford University, Stanford, California 94305, U.S.A.
**Carrick M. Eggleston**
Department of Applied Earth Sciences, Stanford University, Stanford, California 94305, U.S.A.
**Virgil B. Elings**
Digital Instruments Inc., 6780 Cortona Drive, Santa Barbara, California 93117, U.S.A.
**George A. Parks**
Department of Applied Earth Sciences, Stanford University, Stanford, California 94305, U.S.A.
**Gordon E. Brown, Jr.**
Department of Geology, Stanford University, Stanford, California 94305, U.S.A.
**Chao Ming Wu, Kevin Kjoller**
Digital Instruments Inc., 6780 Cortona Drive, Santa Barbara, California 93117, U.S.A.

## Abstract

The atomic structure and nanometer-scale morphology of the (001) surfaces of hematite and galena, exposed by fracturing in air or under oil (to prevent exposure to air) at room temperature, have been studied with scanning tunneling microscopy (STM), low-energy electron diffraction (LEED), and field-emission scanning electron microscopy (FESEM). The (001) surface unit cell of hematite is hexagonal, and the surface diffraction pattern is consistent with the atomic arrangement and cell size of the equivalent plane in the bulk. However, STM has shown that the surface is not flat, but instead consists of undulations, pits, and ridges. The diameters of the undulations range up to several hundred angstroms at their base, with heights between 5 and 100 Å. In places, the surface appears to be atomically flat; however, atomic-resolution images with the STM could not be obtained. The (001) surface unit cell of galena is square, and, as with hematite, the surface diffraction pattern is consistent with the atomic arrangement and cell size of the equivalent plane in the bulk. Direct STM imaging of one-half of the surface atoms (probably S) confirms this result. Lower-resolution STM images again show that the surface is not flat, but consists of irregular undulations (up to 50 Å in height), ridges, and cleavage steps 20 to 50 Å in height. We suggest that the undulations on both the hematite and galena surfaces are mostly the result of uneven fracture propagation due to less than perfect crystallographic control of breakage.

The atomic structure and nanometer-scale morphology of mineral surfaces play a key role in mineral solubility and sorption reactions at the aqueous solution–mineral interface. STM provides a unique means of studying both the structure and the finest-scale morphology of mineral surfaces in vacuum, in air, and under aqueous solution, and it can be used to directly observe and categorize energetically favorable surface sites that are involved in these processes. Electronic and vibrational tunneling spectroscopy, as an extension of STM imaging, is being developed and may be available in the future for identifying individual atoms and molecules on mineral surfaces.

## Introduction

The field of surface science has experienced tremendous growth over the last decade due to significant advances in experimental techniques that provide microscopic details of surfaces. In response to this, an ever-increasing portion of mineralogical research is being devoted to the study of the surfaces of minerals. A thorough knowledge of the physical and chemical properties of mineral surfaces is required to generate a satisfactory understanding of their role in several fundamentally important geochemical processes such as mineral dissolution and precipitation, elemental partitioning at mineral–aqueous solution interfaces, and natural heterogeneous catalytic reactions. Advances in these areas will have pro-

0003–004X/89/1112–1233$02.00

gressively greater impact on more applied fields in the earth sciences, including toxic-waste transport and ore-deposit formation.[1]

Although bulk properties are a function of composition and atomic structure, surface properties depend on composition, structure, *and* morphology. Taking these three factors in turn, surface-sensitive analytic techniques, particularly Auger electron and X-ray photoelectron spectroscopies, have been used for some time to study mineral-surface composition (e.g., see Hochella, 1988). On the other hand, one of the most fundamentally challenging and elusive tasks in the field of surface science has been the determination of atomic structure and subnanometer-scale morphology of solid surfaces. Over the last several decades, low-energy electron diffraction (LEED) has been the primary tool for surface crystallographers (e.g., see Clarke, 1985, and Van Hove et al., 1986), although surface-diffraction information can be difficult to interpret and many surface structures have remained unsolved. The surface crystallography of minerals, as a field of study, is virtually unknown. For the study of surface morphology, the most useful tool has been scanning electron microscopy (SEM), yet this technique lacks the spatial resolution needed to image important fine-scale surface features such as atomic steps, kink sites, defects intersecting or on the surface, and microcracks.

Very recently, scanning tunneling microscopy (STM) has revolutionized the field of surface science by allowing the direct imaging of electronic states on the surfaces of conducting or semiconducting materials with *subangstrom* resolution, essentially allowing the imaging of surface atoms (e.g., see reviews by Golovchenko, 1986, Hansma and Tersoff, 1987, and Hansma et al., 1988). With this important new technique, one can literally view surface atomic structure as well as fine-scale surface morphology, thus effectively overcoming the weaknesses of LEED and SEM. STM has been performed on solid surfaces in vacuum, in air, and under fluids, including water. A related technique, atomic force microscopy (AFM), is currently being developed and has produced atomic-resolution images of insulating surfaces (Binnig et al., 1986; Albrecht and Quate, 1987; Hansma et al., 1988). In addition, AFM has recently been used to image a silicate surface (muscovite) with atomic resolution (Drake et al., 1989).

In this study, we have combined the strengths of STM, LEED, and ultrahigh-resolution field-emission SEM (hereafter referred to as FESEM) in order to characterize the atomic structure and subnanometer-scale morphology of two mineral surfaces, the (001) planes of hematite and galena. These particular minerals were chosen for our first surface structural study because (1) they are both semiconductors, and galena has a particularly narrow band gap, (2) they show well-developed parting, in the case of hematite, and cleavage, in the case of galena, which provides macroscopically flat, and, we hoped, relatively simple surfaces for study, and (3) they are mineralogically important phases and provide us with the opportunity of looking at both an oxide and a sulfide. As we have found, the atomic structures of these surfaces are similar to equivalent atomic planes in the bulk, but the surface morphologies of these supposedly simple and flat surfaces are highly complex and variable.

In the following section, we describe the samples and the techniques used in this study. This description is followed by our observations and interpretations of the structure and morphology of the hematite and galena surfaces. Finally, we discuss our views of the many implications of STM study for improving our understanding of the behavior and role of conducting or semiconducting mineral surfaces in geochemical reactions.

## Experimental details and technique description

### Samples

The hematite and galena specimens used in this study were obtained from the Stanford Mineral Collection. Two Brazilian specular hematite specimens were selected, one from Minas Gerais near Itabira and the other from an unknown locality, which show well-developed (001) parting. Hematite has a band gap of approximately 2.2 eV (Adler, 1968; Quinn et al., 1976). The galena specimens are large euhedral crystals from Northampton, Australia. The perfect cubic cleavage resulted in fracture-exposed flat areas of only a few square millimeters in area, but this was sufficient for all analyses. Galena has a band gap of 0.4 eV (Tossell and Vaughan, 1987, and references therein).

### Scanning tunneling microscopy (STM)

The scanning tunneling microscope consists of an extremely sharp metallic tip that is moved over the surface of interest with a ceramic piezoelectric translator. These translators are controllable to better than 0.1 Å in $x$, $y$, and $z$. When the tip approaches the surface of a conducting or semiconducting sample and is electrically biased by a few millivolts to a few volts relative to the sample, there is some probability that electrons will tunnel across the gap, resulting in a small but measurable current. This tunneling current is extremely sensitive to the separation between the tip and sample, as was first predicted by Frenkel (1930) and first experimentally demonstrated in vacuum by Binnig et al. (1982a).[2] In the

[1] *Editor's note*: The Mineralogical Society of America will hold a short course entitled "Mineral-Water Interface Geochemistry" in conjunction with the 1990 GSA meeting in Dallas, Texas. This course will cover many of the topics alluded to in this article. The course is being convened by M. F. Hochella, Jr., and A. F. White, and the dates are October 26–28, 1990. Detailed information about this course will appear in future issues of the "Lattice."

[2] It is interesting to note that the first atomic-resolution images obtained by an STM were collected on the (110) surfaces of $CaIrSn_4$ and Au (Binnig et al., 1982b) and the (111) surface of Si (Binnig et al., 1983). Gerd Binnig and Heinrich Rohrer won the 1986

simplest one-dimensional treatment, the tunneling current $I_T$ is given by

$$I_T \propto \exp[(-4s\pi/h)(2m\phi)^{1/2}], \quad (1)$$

where $s$ is the barrier width, equivalent to the shortest distance between the sample surface and the end of the tip, $h$ is Planck's constant, $m$ is the electron mass, and $\phi$ is the barrier height, equivalent to the local work function. In practice, the tunneling current can change by a factor of 2 or more with a change in the separation between the tip and the sample of only 1 Å. Therefore, if the tunneling current is kept constant by adjusting $z$ during an $x/y$ scan (the constant-current mode of microscope operation), a three-dimensional "image" with exceptionally high spatial resolution can be generated for the surface of the sample. The image resolution is subatomic in $x$ and $y$, and on the order of 0.1 Å in $z$.

In order to interpret atomic-resolution STM images, it is necessary to more carefully consider the physics of tunneling and the meaning of $s$, the separation between the tip and sample. Tunneling actually occurs between electronic states within a very narrow energy range around the Fermi level of atoms on the sample surface and the end of the tip. Because the tunneling current is so sensitive to $s$, the atom that terminates a sharp tip is the only one that need be considered on the electrode side. The theoretical treatment of tunneling imaging may be accomplished realistically, and greatly simplified, if the tip is therefore treated as a point probe that remains physically unaffected during a scan. In this case, only the electronic properties of the surface atoms of the sample are considered, and under the limit of low voltage and temperature, Tersoff and Hamann (1985) suggested that

$$I_T \propto \sum_{\nu} |\psi_\nu(\mathbf{r}_t)|^2 \delta(E_\nu - E_F), \quad (2)$$

where $\nu$ represents all electron energy levels near the Fermi energy unique to the surface atoms (referred to as surface states), $\psi_\nu$ is a wave function representing each surface state, $\mathbf{r}_t$ is the position of the tip, $E_\nu$ is the energy of each surface state, and $E_F$ is the energy of the Fermi level. The Kronecker delta function $\delta(E_\nu - E_F)$ is essentially 0 when $E_\nu \neq E_F$ and 1 when $E_\nu = E_F$. Therefore, the tunneling current is a function of the local density of states (LDOS), or the charge density, at or very near the Fermi level at the position on the surface where tunneling is taking place into or out of the substrate (this is true whether the substrate is a conductor or a semiconductor). Thus, if $I_T$ is kept constant as the tip is scanned across the surface by continuously adjusting the separation between the tip and sample (constant-current mode), a map of the surface results. This is *not* a direct map of atomic positions, but a relief map of surface LDOS at or near (depending on bias voltage) the Fermi level. However, at atomic resolution, peaks in these maps can represent atomic positions; valleys or saddles can also represent atomic positions if tunneling to or from energy levels localized on these atoms is weak.

The scanning tunneling micrographs shown in this paper were taken with a Digital Instruments NanoScope II tunneling microscope. A W tip (prepared by electrochemical etching in a 1$M$ KOH solution) was used to acquire the atomic-resolution images on the galena surface. All other tunneling images presented in this study were collected using a Pt-Ir tip (prepared by mechanical cutting). To eliminate exposure of the surface to be studied to air, each sample was broken under silicone oil (Dow Corning 704 diffusion-pump oil). The oil-covered sample was transferred to the tunneling microscope, and the tip lowered through the oil until tunneling current was established. Schneir and Hansma (1987) have clearly shown that atomic-resolution tunneling microscopy can be achieved on surfaces under nonpolar liquids, including silicone oil. Scans were made over square areas in the range of 10 nm$^2$ to $10^6$ nm$^2$ and could each be collected in several seconds to several tens of seconds depending on the scan size and the number of lines (or sweeps) per scan. Positive and negative tip biases were used, and the bias voltages ranged from as low as 16 mV for the galena samples to as high as 1500 mV for the hematite. Imaging was performed in the constant-current mode with tunneling currents set between 0.33 and 2.0 nA. Images shown in this paper were stable and reproducible except during periods of thermal drift when images could shift by up to several angstroms per second. Images were collected only during thermally stable periods.

### Field-emission SEM (FESEM)

FESEM differs from conventional SEM primarily because of the addition of a field-emission electron source consisting of an extremely fine single-crystal W tip (cathode) and two anodes. Electrons are extracted from the tip at room temperature by a large field gradient and accelerated down the electron column. A Hitachi S-800 FESEM was used in this study because it is capable of extremely high image resolution (compared with a SEM equipped with thermionic $LaB_6$ and W-filament electron sources), even at low accelerating voltages and on uncoated samples. Conductive coatings, applied to a surface for the purposes of electron-charge neutralization, modify the morphology of surfaces on a very fine scale; this is obviously a problem at extremely high magnifications. In addition, high accelerating voltages can result in electron-beam damage and charging of uncoated insulating samples. At low accelerating voltages (1 to 3 kV), both of these problems can be minimized or eliminated (Hochella et al., 1986). In this study, however, low accelerating voltages were not necessary owing to the semiconducting nature of the samples and their durability under high beam voltages. Thus, we were able to take advantage of the 20-Å lateral resolution that the Hitachi S-800 FESEM can provide at 25 kV. Unfortunately, higher primary voltages

Nobel Prize in physics only four years after inventing this powerful new microscope.

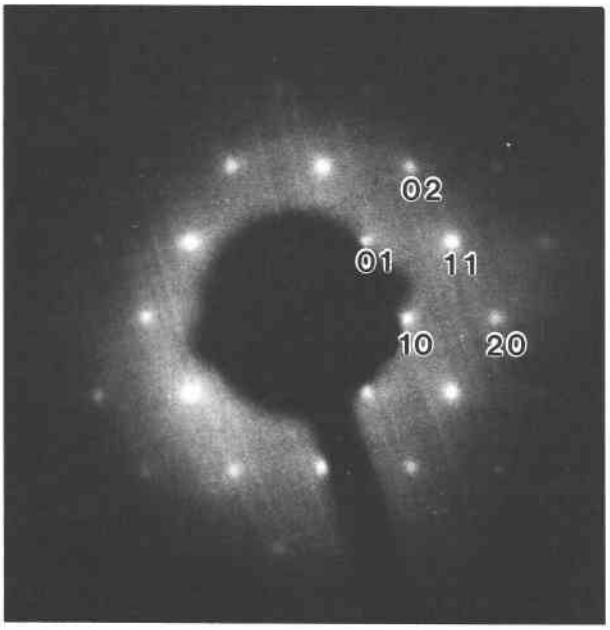


Fig. 1. Indexed low-energy electron-diffraction (LEED) pattern of the hematite (001) surface collected at a primary beam energy of 90 eV. The shadow blocking the view of the direct beam and several diffracted beams is due to the miniature electron gun mounted just above the sample.

also generate secondary electrons that come from deeper in the sample, slightly degrading the detail of the surface image.

### Low-energy electron diffraction (LEED)

The LEED instrument used in this study was a VG model 640-2 RVL reverse-view system mounted on a VG ESCALAB ultrahigh-vacuum chamber. The miniature electron gun in this system has a beam diameter of approximately 0.5 mm.

LEED is performed with a beam of monoenergetic low-energy electrons, most commonly between 30 and 200 eV, impinging on a solid surface typically in the direction normal to the surface plane. A few percent of the incident electrons are elastically backscattered. If the surface atoms are well ordered, coherent diffraction occurs, and a diffraction pattern can be viewed on a hemispherical fluorescent screen above the sample. The diffraction physics is analogous to that in transmission X-ray and high-energy electron diffraction. However, because low-energy electrons travel such short distances through condensed matter owing to phonon and plasmon losses and electron-electron collisions (e.g., Hochella and Carim, 1988), the information in the LEED pattern is generally only from the top few layers of atoms. Therefore, LEED may be regarded as a tool for near-surface atomic-structure analysis.

The near-surface atomic structure is determined by modeling the intensity change of the Bragg reflections (and additional peaks due to multiple scattering) as a function of incident-beam energy via dynamical theory (e.g., see Clarke, 1985). LEED is more routinely used in a less-quantitative mode, as in this study, to determine whether surfaces are crystalline (i.e., whether a pattern can be obtained), and if so, to determine the size and shape of the unit cell in the surface plane. Repeat distances in direct space can be determined with the equation

$$d_{hk} = 66\lambda/p_{hk}, \tag{3}$$

where $d_{hk}$ is the perpendicular spacing of $hk$ lines on the surface in angstroms, 66 is the distance in millimeters from the sample surface to the fluorescent screen in our LEED system, $p_{hk}$ is the distance between reciprocal lattice points measured directly off the film in millimeters (allowances are made for the scale change from the fluorescent screen to the photographic print of the screen), and $\lambda$ is the wavelength of the incident electrons in angstroms. $\lambda$ is calculated from the relativistically corrected de-Broglie equation

$$\lambda = h/[2m_0Ee(1 + Ee/2m_0c^2)]^{1/2}, \tag{4}$$

where $m_0$ is the electron rest mass in kilograms, $E$ is the acceleration voltage of the electron beam in electron volts, $e$ is the electron charge in coulombs, $c$ is the velocity of light in meters per second, and $h$ is Planck's constant in joule seconds. With the substitution of constants, and at the low accelerating voltages used for LEED, Equation 4 simplifies to

$$\lambda = (150.4/E)^{1/2}. \tag{5}$$

Finally, $d_{hk}$ is converted into a unit-cell edge. The uncertainty in the cell-edge measurement is due to the width of the diffracted spots, the fact that reciprocal space is slightly distorted on the fluorescent screen, and the inaccuracy in measuring the scale change from the actual pattern to the photographic reproduction. It is estimated that these errors result in an uncertainty in cell-edge measurement of $\pm 1\%$.

## Results and discussion

### Hematite

Hematite is hexagonal, and its bulk structure can be described as a slightly distorted, closest-packed array of oxygens with Fe filling two-thirds of the octahedral sites. The LEED pattern obtained from the hematite (001) surface is shown in Figure 1. This hexagonal pattern was consistently observed over the surfaces of both hematite samples. There are no systematic absences in this pattern (see below for explanation), and the method described above for determining the surface unit-cell dimensions gives $a_1 = a_2 = 5.07$ Å, which agrees within error with the known $a$ cell edge of 5.04 Å measured from the bulk sample. This strongly suggests that the (001) surface of hematite exposed by fracturing in air at room temperature maintains a structure very similar to that of the equivalent plane in the bulk sample.

It should be noted that Kurtz and Henrich (1983) have used LEED to study the structure of the (001) surface of

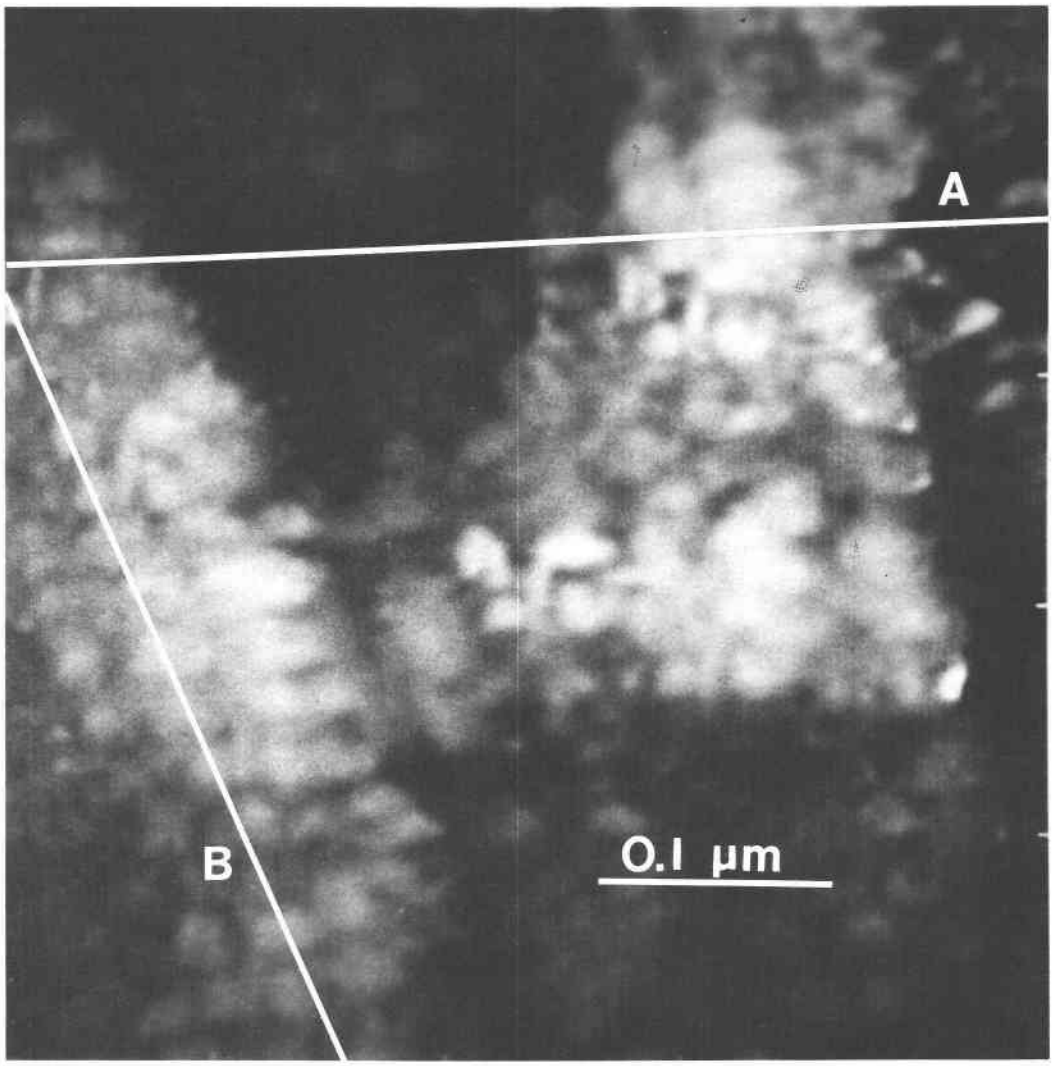


Fig. 2. Scanning-tunneling-microscope (STM) image of the (001) surface of hematite viewed perpendicular to the surface. This image was taken with a tip bias of −1500 mV and a tunneling current of 2.0 nA. At this scale, the STM is mapping the surface topography as indicated by the gray-scale coloration of the image from white (highest points) to black (lowest points). Cross sections along lines A and B are shown in Fig. 3.

hematite upon heating. Although they started with a (001) surface that was ion-bombarded and therefore made nonstoichiometric and amorphous (Hochella et al., 1988b), they found that heating to 700 °C produces a hexagonal, stoichiometric surface reconstruction with a unit cell of twice the dimensions of the one we have observed. Further, heating to 820 °C produces an ordered but incommensurate overlayer whose structure has yet to be determined. Because Kurtz and Henrich (1983) did not observe an ordering of the amorphous iron oxide surface until a high temperature was reached, it is likely that the bulklike structure that we observed at room temperature on a freshly fractured surface will also be stable to relatively high temperatures, at least in a vacuum. Reconstruction of the surface will probably occur at lower temperatures when in contact with air or an aqueous solution (e.g., see Onoda and DeBruyn, 1966).

Additional understanding of the hematite LEED pattern can be obtained by considering the depth in the sample from which the pattern is generated. From studies of electron-attenuation length such as those by Seah and Dench (1979) and Hochella and Carim (1988), we can estimate that two-thirds of the peak intensity in a hematite LEED pattern collected near 100-eV beam energy (actual patterns were collected between 90 and 115 eV) comes from within approximately 3 Å of the surface and that 95% comes from within approximately 8 Å of the surface. These depths are much less than the unit-cell length in this direction in the hematite structure ($c$ = 13.75 Å), so we can expect the symmetry of the LEED pattern to be

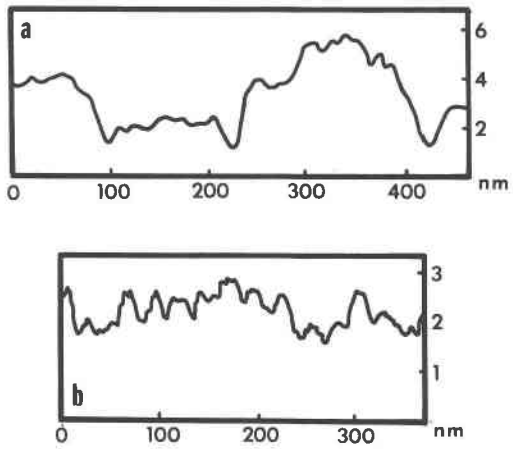


Fig. 3. Cross sections through the STM image shown in Fig. 2. The left sides of these profiles (labeled a and b) correspond with the left sides of the lines in Fig. 2 (labeled A and B). Note the large vertical exaggeration.

based only on the two-dimensional nature of the top few atomic monolayers. The two-dimensional space group (plane group) of the hematite (001) surface is $p31m$, which has no conditions limiting possible reflections. Therefore, we expect no systematic absences in the LEED pattern of the hematite (001).

A low-resolution STM image of the hematite surface is shown in Figure 2 along with two corresponding profiles in Figures 3a and 3b. This type of surface, in places showing fairly regular linear arrays of undulations, is typical of several (001) surfaces of both hematites examined in this study. The profile in Figure 3b clearly shows that the undulations are 200 to 300 Å in diameter and generally between 4 and 6 Å in height. The profile in Figure 3a shows broader-level changes on the hematite surface, with one depression generally 20 to 30 Å deep with a lateral extent on the order of 1000 Å. Figure 4 is another low-resolution STM image of the hematite (001) surface showing different morphology. In this image, the undulations are not in linear arrays, but the relief is greater, with mounds raising up to as high as 100 Å with diameters at their bases still in the 200- to 300-Å range. We did not observe sharp atomic steps or microcracks in any of the STM images of the hematite (001).

Figure 5 is an ultrahigh-magnification, high-resolution SEM image of the hematite surface showing apparent mounds with similar width, spacing, and neighboring flat regions as revealed in the STM image shown in Figure 4. A careful comparison of these STM and FESEM images is

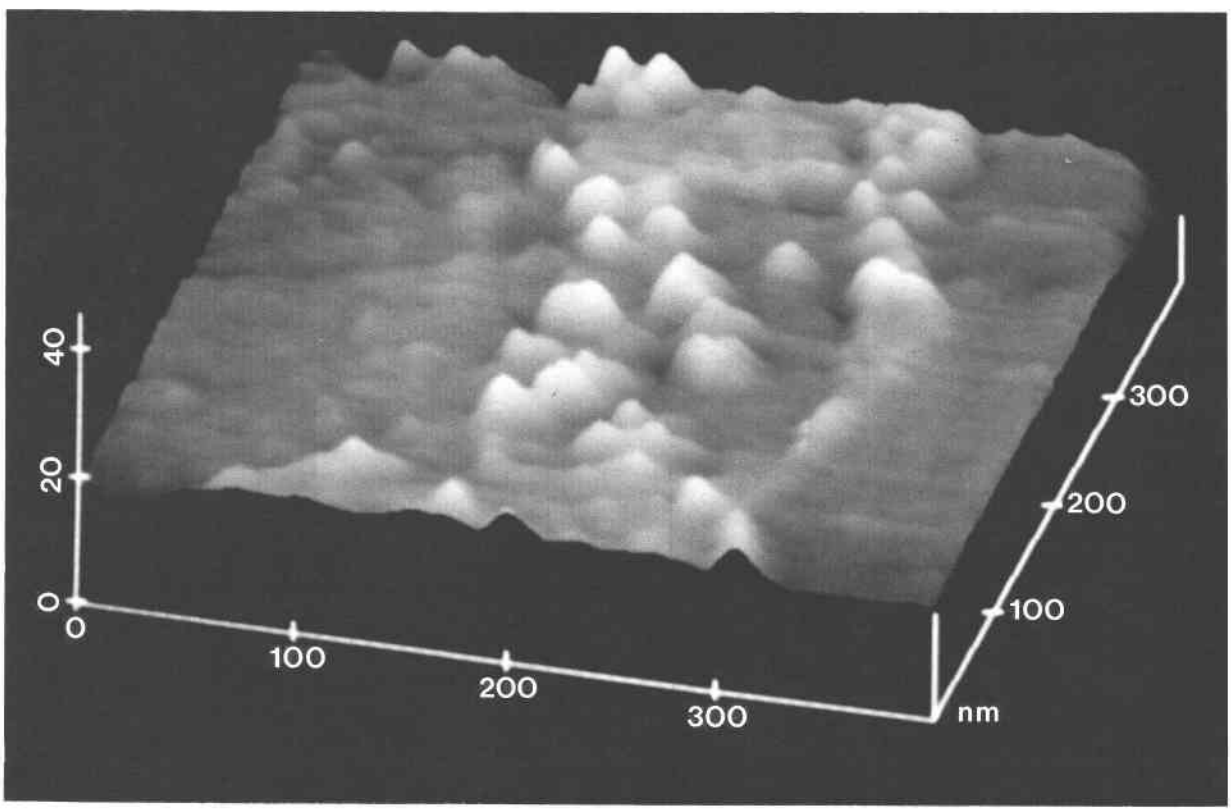


Fig. 4. Side view of an STM image of the (001) surface of hematite showing moderate vertical exaggeration. This image was taken with a tip bias of −1500 mV and a tunneling current of 2.0 nA. The undulations running through the center of the image (up to 100 Å in height) are flanked on both sides by atomically smooth areas.

important for two reasons. First, the FESEM image gives direct evidence that the STM images are not the result of instrumental artifacts or the presence of the overlying oil. The surface imaged by the FESEM was simply exposed by fracturing in air and immediately placed into the high vacuum of the instrument. In addition and as mentioned earlier, Schneir and Hansma (1987) have shown that STM images of the surfaces of graphite, GaAs, and a Au film deposited on a glass substrate are not affected when covered with nonpolar liquids including silicone oil. Second, a comparison of the two images demonstrates the dramatic capabilities of the STM in both lateral and height resolution even for relatively wide scans. Further, the smaller undulations detected by STM (Fig. 2) are well beyond the imaging resolution of SEM.

The reason for the undulations seen on both hematite samples is not known. Speculation on their origin is confounded by the fact that, in some areas, they appear to be arranged in linear arrays (Fig. 2), whereas in other areas, they are more randomly distributed (Figs. 4 and 5). Also, as stated previously, their heights are quite variable. To our knowledge, this type of undulation has never before been seen in bulk (TEM) studies of hematite. In addition, there is no known structural mechanism in hematite, such as a dimensional misfit between adjacent polyhedral layers, that should cause lattice distortion and bending as seen, for example, in chrysotile (Yada, 1967, 1971; Veblen and Buseck, 1979). Therefore, for now we will assume that this feature is strictly a surface-related phenomenon, and we will briefly consider two possibilities for its origin. We first consider the possibility that the undulations occur immediately after fracture because of structural relaxation. LEED clearly shows that the surface unit cell is the same size as the equivalent in the bulk, but surface relaxation will most likely occur by the contraction of the top few atomic layers in the direction perpendicular to the surface (see Somorjai, 1981, for a compilation of such data for certain metals, alloys, and oxides). Such a contraction might result in the features seen if it is not uniform owing to surface inhomogeneities (compositional, surface defects, etc.). To test this hypothesis, the surface compositions of the two hematite specimens used for STM imaging were measured with X-ray photoelectron spectroscopy (XPS). Although Al was present in the near-surface of one of the samples, the other showed only Fe and oxygen. This latter observation, combined with the high quality of the hematite LEED patterns, indicates that at least this sample has a stoichiometric surface, yet it still shows undulations in STM images. Also, the density of bulk defects intersecting the surface (expected to be in the range of $10^{-5}$/cm$^2$ to $10^{-9}$/cm$^2$ for most minerals; e.g., see Brantley et al., 1986, Lasaga and Blum, 1986, and Schott et al., 1989) is many orders of magnitude too low to account for the close spacing of undulations as seen, for example, in Figure 2. Finally, we do not believe that surface relaxation alone could result in such large undulations when this phenomenon is generally measured in small fractions of unit-cell edges

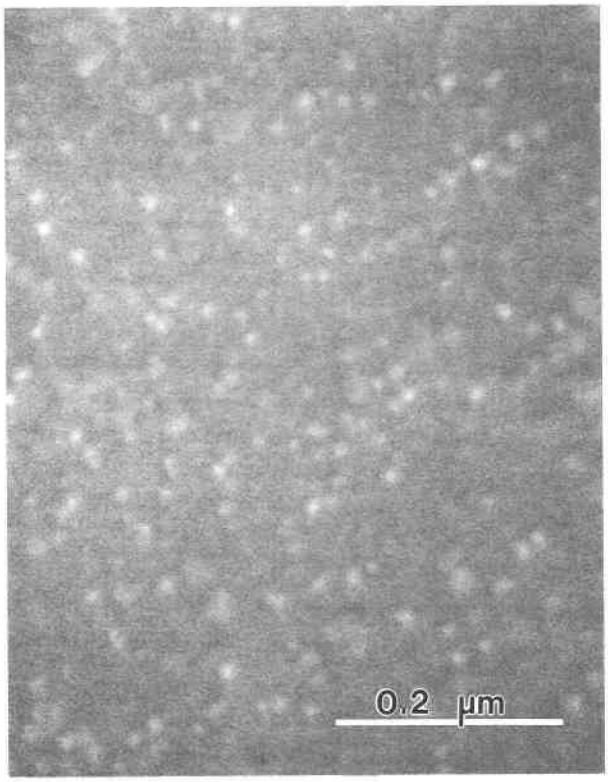


Fig. 5. Ultrahigh-magnification field-emission scanning-electron-microscope (FESEM) image of the (001) surface of hematite taken at 25 kV. Note the general similarity in the width and distribution of the apparent mounds in this image with the STM image in Fig. 4, keeping in mind the difference in scale (0.2 $\mu$m = 200 nm).

(Somorjai, 1981). Therefore, at the present time, we consider surface relaxation to be an unlikely possibility for the origin of the hematite (001) surface morphology.

The other possibility that might explain the presence of the undulated surface simply relates to a fracture effect. Micrometer- to millimeter-sized morphological features due to fracture of both crystalline and amorphous materials can be highly complex and variable (e.g., see Lawn and Wilshaw, 1975). The hematite (001) fracture plane is along parting, and the breakage may not take place along a single atomic plane. The undulations may not be atomically smooth mounds, but in fact consist of a series of atomic steps that result in moundlike features. Atomic steps have been imaged with STM (e.g., Golovchenko, 1986; Zheng et al., 1988), and more high-resolution STM imaging is needed on the hematite surface to explore this possibility further. STM may be able to document on the atomic level the fracture pattern that results in the surface morphology seen.

In Figure 4, the areas with mounds are flanked by areas that appear to be atomically flat. It is in these areas where we attempted to perform atomic-resolution STM with various tunneling currents and using both positive and neg-

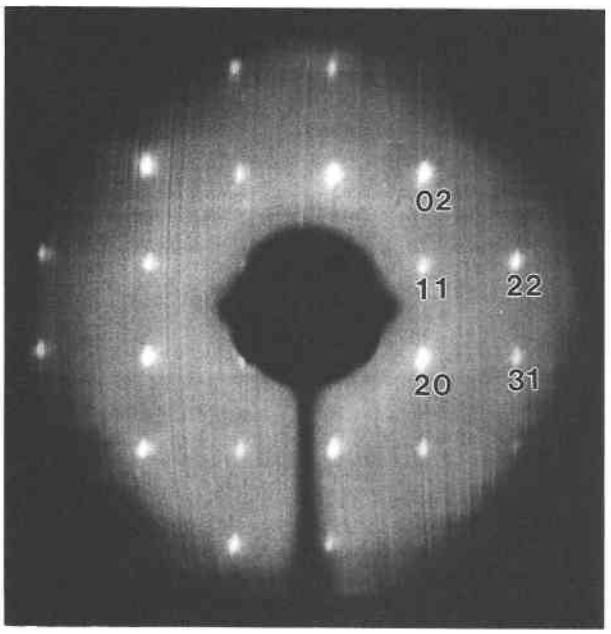


Fig. 6. Indexed low-energy electron-diffraction (LEED) pattern of the galena {001} surface collected at a primary beam energy of 98 eV.

ative tip biasing. However, we were unsuccessful in obtaining regular arrays of peaks even though LEED clearly indicates that the surface is ordered. The reason for our inability to obtain atomic-resolution images of the hematite (001) surface is not known. As mentioned previously, a relatively large bias voltage was needed to establish a tunneling current that was continuous and steady enough to obtain relatively low resolution STM images. However, atomic-resolution images have been obtained before at these and even higher bias voltages (e.g., Binnig et al., 1983). Perhaps, with a band gap of over 2 eV and with the possibility of the Fermi level in pure $Fe_2O_3$ residing near midgap, tunneling involving either valence or conduction states at the bias voltages used does not have the stability required to generate atomic-resolution images.

### Galena

The LEED pattern of a galena {001} surface can be quite complex, at least in part because of our inability to obtain a freshly fractured galena surface without numerous steps as a result of its three perfect directions of cleavage. However, macroscopically flat areas often give simple square LEED patterns, as shown in Figure 6. Galena has the NaCl structure, and the ideal (unreconstructed) galena {001} surface will have a square unit cell with S (or Pb) at the corners and in the center, and Pb (or S) halfway along each edge. The plane-group symmetry for this arrangement is *p4g*, and with S at 0,0 and Pb at ½,0, the special condition *hk*: $h + k = 2n$ limiting possible reflections applies. Therefore, the LEED pattern shown in Figure 6 is actually a centered square pattern as shown, and the *a* cell edge measured from this pattern is 6.00 Å. This value is in agreement, within error, of the known *a* cell edge of 5.94 Å measured from the bulk sample. Therefore, it is likely that this surface has not reconstructed or become structurally distorted after fracture and exposure to air at room temperature.

A low-resolution STM image of the galena surface is shown Figure 7. This image, 2000 Å on a side with moderate vertical exaggeration, shows that the "perfect" cleavage surfaces of galena are far from flat on an atomic scale. The sharp ridge marked on the figure, probably representing a cleavage step with at least two kink sites visible, has a vertical relief of 30 to 50 Å. The terraces between ridges have undulations that do not appear to follow any particular pattern, and the local vertical relief on these terraces is generally between 5 and 30 Å. At higher resolution on a relatively flat area (Fig. 8), a periodic array of peaks can be seen with a separation along a row of approximately 4.0 Å. The nearest-neighbor Pb-Pb and S-S distances on the galena {001} are 4.2 Å. The 5% difference in dimension is within the STM *x,y* calibration error (5–10%), so it is straightforward to interpret the peaks seen in this STM image as representing either all of the Pb or all of the S atoms on the {001} surface.

We were only able to obtain STM images of galena with the tip biased negatively, thereby probing empty or partially filled states near the Fermi level of the galena surface atoms. This situation was also encountered by Zheng et al. (1988) in their STM study of the galena surface in vacuum. In addition, observing only half of the atoms on the surface of galena, as we have seen in this study with the sample under oil, has also been seen before with the sample imaged in air (I. Tsong, personal communication). Only imaging galena in vacuum (Zheng et al., 1988) results in images that show both atoms. In this case, one type of atom seems to protrude at the surface. Zheng et al. postulated that the atom "protruding" was S because of its higher density of states near the Fermi level, as predicted for IV–VI semiconductors (Dalven, 1973). Therefore, the atoms seen by STM on the galena surface in air or under oil are most likely the S atoms.

The atomic-resolution STM images of Zheng et al. (1988) and this study clearly confirm the suggestion made by the LEED results presented above that the galena {001} surface, exposed by fracture at room temperature, does not reconstruct. This interpretation seemingly justifies the assumptions made by Tossell and Vaughan (1987) and other workers regarding the structure of the galena surface in their studies of its surface electronic structure and chemical reactivity. However, as with the hematite, we did not generally find an atomically flat surface. As with hematite, we believe that the surface undulations are most likely due to a fracture effect, but this interpretation remains to be fully demonstrated. In any case, the complex surface morphology would certainly be expected to locally influence the electronic structure and reactivity of the surface as described below.

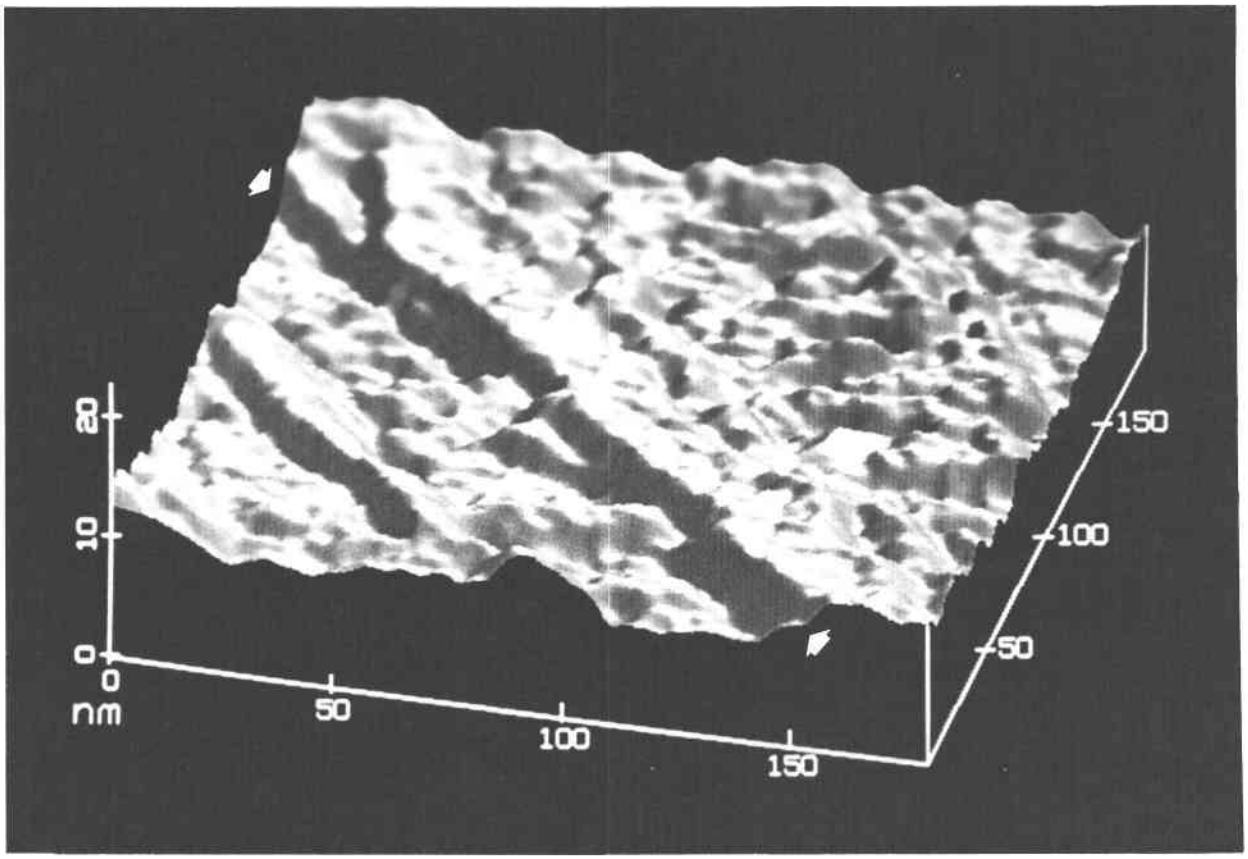


Fig. 7. Side view of an STM image of the galena {001} surface showing moderate vertical exaggeration. This image was taken with a tip bias of −20 mV and a tunneling current of 0.9 nA. The total vertical relief in the upper right quarter of the image is approximately 30 Å. The cleavage step marked by two arrows varies between 30 and 50 Å in height and has two kink sites (re-entrants) along its length.

## IMPLICATIONS

### Sorption at the aqueous solution-mineral interface

The partitioning of ions at a liquid-mineral interface has been an area of intense study for decades owing to the importance of sorption phenomena in many areas of geochemistry, including species mobility in ground water, ore-deposit formation, and mineral growth. The details of the atomic structure of sorption complexes at the aqueous solution–mineral interface are just now being elucidated (e.g., see Hayes et al., 1987). However, surface heterogeneity is rarely considered in sorption studies owing to the lack of information on surface structure and fine-scale morphology. Yet it is very likely that real mineral surfaces are inhomogeneous, as emphasized in this study, and it is likely that this inhomogeneity has an important effect on sorption reactions at the aqueous solution–mineral interface.

The inhomogeneity of surfaces and its effect on sorption are probably nowhere better understood than in gas-solid systems where the solids are simple metals. For example, high-resolution electron-energy-loss spectroscopy indicates that molecular CO will adsorb intact on flat Pt surfaces, but the molecule will dissociate when adsorbed onto step or kink sites (Iwasawa et al., 1976). Certainly, molecular dissociation is one of the keys to heterogeneous catalysis reactions. In addition, there are many cases reported where adsorption probabilities of gases are increased in the presence of surface steps. Examples include $H_2S$ and $O_2$ on Cu (Perdereau and Rhead, 1971) and $H_2$ and $O_2$ on Pt (Christman and Ertl, 1976). Somorjai (1981) has suggested that this effect is due to a reduction of the thermal-activation-energy barrier for bonding at step sites as well as the generally stronger bonding interaction between adsorbates and surface atoms at surface irregularities.

Solution-mineral interactions are chemically more complex and considerably more difficult to study than gas-metal systems; however, there is still a great deal of evidence that surface inhomogeneities play a major role in these sorption processes. Dibble and Tiller (1981) have strongly highlighted the importance of atomic steps, edges, and kink sites in their extensive theoretical treatment of nonequilibrium, interface-controlled, water-rock inter-

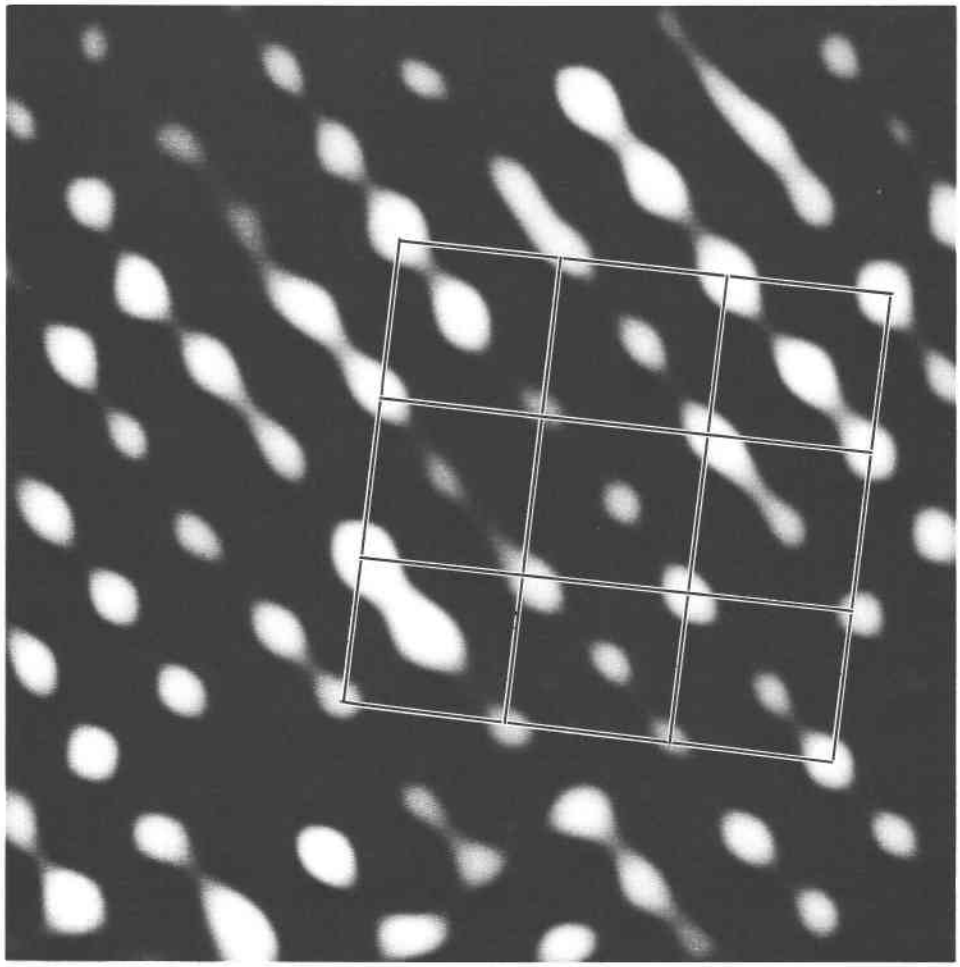

Fig. 8. Atomic-resolution STM image viewed perpendicular to the galena {001} surface. This image was taken with a tip bias of −25 mV and a tunneling current of 2.4 nA. The regular array of bright spots probably represents surface S atoms (see text). Nine surface unit cells, with S atoms at 0,0 and ½,½, are marked. The unit cell edge is 5.9 Å. The diagonal streaking in the image (from upper left to lower right) is a scanning artifact.

actions. They have even suggested that surface reconstruction or edge and step formation may be the dominating factor in controlling many solution-mineral interactions. Experiments involving the adsorption of Cd, Cu, Zn, and Pb on amorphous iron oxyhydroxides by Benjamin and Leckie (1981a, 1981b) and Pb on goethite by Hayes and Leckie (1986) suggest a surface with many discrete sites for sorption, each with a different binding strength for different sorbates. Several other workers—such as Loganathan and Burau (1973) and Guy et al. (1975), who studied the adsorption of various cations onto $MnO_2$—suggest that multiple sorption sites exist on mineral surfaces. Infrared (IR) spectroscopy studies (e.g., Parfitt and Russell, 1977) have been particularly helpful in identifying the different types of hydroxyl groups present on oxide surfaces, again implying the existence of multiple discrete sites for sorption reactions. In addition, direct observation can sometimes suggest surface sorption inhomogeneity. For example, in experiments involving the reduction and adsorption of Au from solution onto sulfide surfaces (Jean and Bancroft, 1985; Hyland and Bancroft, 1989), SEM observation shows that the Au agglomerates that grow on the surface with time seem to nucleate on steps and edges. This observation suggests that the first sorption reactions preferentially occurred at these sites. Another example of the direct observation of sorption-site heterogeneity can be found in a study of the partitioning of uranyl cations at the aqueous solution–mica interface (Lee and Jackson, 1977). By using the $^{235}U$ fission-particle-track method, it was found that uranyl complexes preferentially adsorb at crystal edges and optically visible steps.

STM of the hematite and galena (001) surfaces clearly shows a great deal of inhomogeneity and irregularity that should affect sorption behavior. Inhomogeneity is apparent at the nanometer scale (Figs. 2, 4, and 7) as well as

at the atomic scale (Fig. 8). Both STM and AFM will be excellent tools for characterizing these irregular features on surfaces so that changes in sorption behavior can be more clearly correlated with surface form. In addition, it may be possible to image sorption complexes at the solution-mineral interface in situ with STM and AFM.

### Mineral solubility

The solubility of silicate minerals in aqueous solutions has received a tremendous amount of renewed interest in just the past few years (e.g., see Knauss and Wolery, 1986; Petit et al., 1987; Hochella et al., 1988a; Muir et al., 1989; Casey et al., 1988, 1989). As Eggleston et al. (1989) have pointed out, the dissolution behavior of minerals is complicated by many factors both intrinsic and external to the dissolving phase. One of the intrinsic factors is the shape of its surface. This fact was first recognized some time ago when it was observed that finely divided particles have an increased solubility over larger particles of the same material (e.g., see Enustun and Turkevich, 1960, and references therein). This phenomenon can be described by using a modified version of the Kelvin equation (originally written for the liquid-gas interface to describe the change in vapor pressure for a curved surface) as follows:

$$S/S_0 = \exp[(2\gamma\bar{V})/(RTr)], \tag{6}$$

where $S$ is the solubility of grains with inscribed radius $r$, $S_0$ is the bulk solubility, $\gamma$ is the interface free energy, $\bar{V}$ is the molar volume of the solid, $R$ is the gas constant, and $T$ is the absolute temperature (see also Holdren and Berner, 1979, and Petrovich, 1981). Considering now the effect of surface roughness on solubility instead of particle size, $S$ would be the local solubility of some feature on a surface with inscribed radius $r$, and $S_0$ would be the solubility of an atomically flat surface. All that is needed to estimate the increase in solubility of a small radius-of-curvature feature is the interfacial free energy. These energies have been measured or estimated to be on the order of a hundred to a few hundred millijoules per square meter for several silicate minerals in aqueous solution (e.g., Schultz et al., 1977a, 1977b; Iler, 1980; Petrovich, 1981; Parks, 1984). Therefore, at room temperature, a surface feature with an $r$ of a few hundred angstroms would have a solubility significantly greater than a flat surface (approximately double), and for a feature with an $r$ of only several tens of angstroms, the solubility would be over an order of magnitude greater.

In addition to the above, theory has long predicted, and experimental work has often suggested, that detachment reactions will occur preferentially at high-energy sites, including steps, kinks, edges, defect outcrops, microcracks, etc. Recently developed theory (e.g., Lasaga and Blum, 1986) and some of the latest experimental work (e.g., Holdren and Speyer, 1985, 1987; Brantley et al., 1986) have helped to clarify and quantify this notion. In this regard, Schott et al. (1989) have recently suggested that for strained calcite, more detachment reactions occur at edges and steps than at defect outcrops.

STM and AFM should be ideal tools for measuring and understanding the effects of general surface roughness and specific high-energy sites on solubility. Not only can these features be seen with tunneling or force microscopy, but it should be possible to follow the evolution of these features (e.g., etch pits) during dissolution by performing time-lapse studies under water. In effect, the change in shape of different surface features (steps, kinks, edges, points, etc.) could be followed in real time during dissolution, and their effect on the macroscopically observed solubility calculated.

### Surface energy and fracture propagation

The phenomena discussed above include in their treatment a surface-energy term. The ability to directly observe the atomic-scale surface structure of materials provides a method for investigating structural aspects of the fundamental concept of surface energy. The creation of new solid-surface area, whether by nucleation and growth or by fracture, requires energy input. The surface free energy, $\gamma$, of a solid is defined as

$$\gamma = (\partial G/\partial A)_{P,T,n}, \tag{7}$$

where $G$ is the Gibbs free energy, $A$ is the surface area, and the subscript $n$ requires invariant composition in the bulk and on the surface (see Adamson, 1982, or Parks, 1984). The surface energy varies with the chemical environment of the surface according to the relation

$$d\gamma = -\sum_i \Gamma_i d\mu_i \tag{8}$$

for all species $i$ interacting with the surface, where $\Gamma$ is the adsorption density and $\mu$ is the chemical potential. Using these relations, we might anticipate that surface energy depends on the surface arrangement of atoms. To illustrate this, we may visualize the creation of a surface, say by fracture, in two steps: (1) the separation of a three-dimensional structure along a plane and (2) relaxation of the surface to a structure reflecting the asymmetrical bonding environment of the surface (e.g., Benson and Yun, 1967). During step 1, bonds extending across the plane of the surface must be broken, which requires a certain amount of energy. Under ideal circumstances, then, the energy required to propagate a fracture can be equated with $2\gamma$ according to Equation 7. In practice, however, $\gamma$ will differ from the fracture-propagation energy because the surface created may not be at "equilibrium," and surface relaxation or reconstruction (rearrangement of atoms) or chemical interaction with the environment will ensue, changing $\gamma$ via the thermodynamic and composition terms in Equation 8.

In this study we have been able to show, using STM and LEED, that the hematite and galena surfaces do not undergo surface reconstruction after fracture, although relaxation mechanisms perpendicular to the surface plane cannot be ruled out. Thus, reconstruction and relaxation in the sur-

face plane do not contribute to $\gamma$ under the conditions of our samples. In any case, these methods will provide some insight into the structural basis for surface energy, changes in surface energy, and changes in surface reactivity.

An interesting area of application in this regard might be the study of fracture propagation, a process that has great importance not only in industry (strength of materials), but also in geology (the development of fracture systems in rock). Chemical agents that reduce surface energy (e.g., water interacting with silica surfaces; see Parks, 1984) also reduce fracture-propagation energies (e.g., silica fracture in water; see Michalske and Freiman, 1983). For silicas it is thought (Michalske and Freiman, 1983; Michalske and Bunker, 1984) that interaction of water with strained Si-O-Si linkages at the crack tip accelerates fracture. Direct STM or AFM observation of crack tips intersecting surfaces might provide a way of elucidating fracture mechanisms, perhaps by detecting changes in crack-tip dimensions or shape induced by changes in chemical environment.

### Tunneling electronic and vibrational spectroscopy

The use of STM in surface characterization of conducting or semiconducting minerals goes beyond the more obvious applications of structural and morphological studies already presented. STM can also be used for electronic and vibrational spectroscopy. For electronic spectroscopy, it is important to consider, as mentioned above, that STM does not result in a map of atomic positions, but a map of the surface's local density of electronic states near the Fermi level. With the tip biased negatively, tunneling will occur most readily to surface atoms that have a high density of unoccupied states (therefore, the tip will move away from the surface in the constant-current mode, resulting in a peak in the STM map); in contrast, a positively biased tip will result in a higher tunneling current to surface atoms that have a high density of occupied states (again, in the constant-current mode, the tip will move away from the surface). If theory can be used to predict the localization of occupied and unoccupied states on certain surface atoms, atoms can be differentiated by type in STM maps. Although the imaging of galena in this study provides a partial example of the above principles, a complete example can be found in the atom-selective STM imaging of the GaAs(110) surface by Feenstra et al. (1987). In their study, it was shown that either all of the Ga or all of the As surface atoms can be imaged depending on whether the tip is biased positively or negatively. Obviously, the electronic implications of STM maps will be very useful in the future for identifying atoms on mineral surfaces.

STM also has vibrational spectroscopic capabilities that could be used in the future to characterize and even identify surface atoms and atomic clusters or molecules. This type of tunneling spectroscopy will be possible when it is more fully understood how tunneling electrons interact with vibrational modes of, for example, a molecule attached to a surface. The advantage of this type of vibrational spectroscopy is that the vibrational modes of individual molecules can be explored. Although selection rules have yet to be deduced, certain workers have already shown qualitative success with the technique. For example, Smith et al. (1987) have detected the change in tunneling current as a function of varying bias voltage with the tip stationary over a single sorbic acid molecule supported on a graphite substrate. A plot of $dI/dV$ vs. $V$ (where $I$ is the tunneling current and $V$ is the bias voltage) results in a spectrum of well-defined peaks whose energies correspond to the known vibrational frequencies of this molecule. Studies of this type should provide a foundation for a powerful new auxiliary technique to imaging STM.

## Summary

In this study, we have combined an important new imaging technique, scanning tunneling microscopy, with low-energy electron diffraction and field-emission scanning electron microscopy to study the crystallography and morphology of the hematite and galena (001) surfaces. These surfaces, exposed by fracturing in air or under oil at room temperature, do not reconstruct and have the same atomic structure as the equivalent plane in the bulk structure. Undulations on both surfaces generally have dimensions of approximately 100 to 400 Å in diameter at the base and 5 Å (on hematite) to 30 Å (on galena) in height. A few undulations seen on the hematite surface have a vertical relief of up to 100 Å. In addition to undulations, relief on hematite is seen in the form of pits and ridges with vertical relief of several tens of angstroms, and 30- to 50-Å cleavage steps are readily apparent on the galena surface.

Although the hematite and galena structures do not relax significantly in the plane of the fracture, they may relax perpendicular to this plane. If this relaxation is inhomogeneous because of structural defects and/or compositional variations, it could result in the undulations seen on both surfaces. However, we have found a sample of an undulated hematite surface that is also stoichiometric. In addition, defect densities in minerals are not nearly high enough to cause such closely spaced undulations. On the other hand, it seems much more likely that the undulations are due to an uneven fracture propagation (or less than perfect crystallographic control of breakage) on a very fine scale.

Atomic-resolution STM imaging of the hematite (001) surface has not yet been successful, although in principle it should be possible to accomplish. On the other hand, atomic-level imaging of the galena {001} surface has been achieved under nonvacuum conditions. In our STM scans, significant tunneling between one-half of the surface atoms (probably S) and the tip occurred. In this case, the Pb atoms would be represented by valleys in the STM image between adjacent S atoms along a cell edge. These atoms are not "imaged" owing to very small tunneling currents between them and the tip. It is not unusual to "see" only a portion of the surface atoms with STM, de-

pending on the electronic characteristics of the different atoms on the surface.

In general, the properties of surfaces are controlled not only by their composition and atomic structure, but also by their morphology. At less than atomic resolution, STM images can be thought of more simply in terms of Equation 1, and the instrument becomes a relatively simple topographic tool with extremely high spatial resolution and the ability to accurately measure relief. It is clear that STM (and soon AFM) will significantly advance our understanding of nanometer-scale mineral-surface morphology and help quantify the role of morphology in dissolution and sorption reactions. At atomic resolution, STM image interpretation becomes more difficult as suggested by Equation 2. However, with computer-generated image simulation, the addition of tunneling electronic and vibrational spectroscopy, and basic intuition from the principles of tunneling physics, identification of atoms in STM images is becoming more and more routine. With this, the direct and in situ imaging and image interpretation of individual surface-sorption sites and sorbed species, as well as energetically favorable detachment (dissolution) sites, are now within the realm of possibility.

In conclusion, it seems clear that whether using STM as a low-resolution topographic tool, as a high-resolution imager of atomic features, or as an electronic or vibrational spectroscopic device, its further development and application will result in a new or significantly improved understanding of many aspects of mineral-surface geochemistry.

## Acknowledgments

We are indebted to the Center for Materials Research at Stanford for both financial and instrumental support. This study was also supported in part by NSF Grant EAR 8805440. In addition, we are grateful to Ray Browning of the Center for Integrated Systems at Stanford for assistance with the field-emission SEM. G. Michael Bancroft (University of Western Ontario), David Mogk (Montana State University), George Rossman (Caltech), and David Vaughan (University of Manchester) provided thoughtful reviews that improved the manuscript.

## References cited

Adamson, A.W. (1982) Physical chemistry of surfaces (4th edition), 664 p. Wiley, New York.

Adler, D. (1968) Insulating and metallic states in transition metal oxides. In F. Seitz, D. Turnbull, and H. Ehrenreich, Eds., Solid state physics, 21, p. 1–113. Academic Press, New York.

Albrecht, T.R., and Quate, C.F. (1987) Atomic resolution imaging of a nonconductor by atomic force microscopy. Journal of Applied Physics, 62, 2599–2602.

Benjamin, M.M., and Leckie, J.O. (1981a) Multiple-site adsorption of Cd, Cu, Zn, and Pb on amorphous iron oxyhydroxide. Journal of Colloid and Interface Science, 79, 209–221.

——— (1981b) Competitive adsorption of Cd, Cu, Zn, and Pb on amorphous iron oxyhydroxide. Journal of Colloid and Interface Science, 83, 410–419.

Benson, G.C., and Yun, K.S. (1967) Surface energy and surface tension of crystalline solids. In E.A. Flood, Ed., The solid-gas interface, p. 203–269. Marcel Dekker, New York.

Binnig, G., Rohrer, H., Gerber, Ch., and Weibel E. (1982a) Tunneling through a controllable vacuum gap. Applied Physics Letters, 40, 178–180.

——— (1982b) Surface studies by scanning tunneling microscopy. Physical Review Letters, 49, 57–61.

——— (1983) 7 × 7 reconstruction on Si(111) resolved in real space. Physical Review Letters, 50, 120–123.

Binnig, G., Quate, C.F., and Gerber, Ch. (1986) Atomic force microscope. Physics Review Letters, 56, 930–933.

Brantley, S.L., Crane, S.R., Crerar, D.A., Hellmann, R., and Stallard, R. (1986) Dissolution at dislocation etch pits in quartz. Geochimica et Cosmochimica Acta, 50, 2349–2361.

Casey, W.H., Westrich, H.R., and Arnold, G.W. (1988) Surface chemistry of labradorite feldspar reacted with aqueous solutions at pH = 2, 3, and 12. Geochimica et Cosmochimica Acta, 52, 2795–2807.

Casey, W.H., Westrich, H.R., Arnold, G.W., and Banfield, J.F. (1989) The surface chemistry of dissolving labradorite feldspar. Geochimica et Cosmochimica Acta, 53, 821–832.

Christman, K., and Ertl, G. (1976) Interaction of hydrogen with Pt(111): The role of atomic steps. Surface Science, 60, 365–384.

Clarke, L.J. (1985) Surface crystallography, an introduction to low energy electron diffraction, 329 p. Wiley, New York.

Dalven, R. (1973) Electronic structure of PbS, PbSe, and PbTe. In H. Ehrenreich, F. Seitz, and D. Turnbull, Eds., Solid state physics, 179–224. Academic Press, New York.

Dibble, W.E., Jr., and Tiller, W.A. (1981) Non-equilibrium water/rock interactions—I. Model for interface-controlled reactions. Geochimica et Cosmochimica Acta, 45, 79–92.

Drake, B., Prater, C.B., Weisenhorn, A.L., Gould, S.A.C., Albrecht, T.R., Quate, C.F., Cannell, D.S., Hansma, H.G., and Hansma, P.K. (1989) Imaging crystals, polymers, and processes in water with the atomic force microscope. Science, 243, 1586–1589.

Eggleston, C.M., Hochella, M.F., Jr., and Parks, G.A. (1989) Sample preparation and aging effects on the dissolution rate and surface composition of diopside. Geochimica et Cosmochimica Acta, 53, 797–804.

Enustun, B.V., and Turkevich, J. (1960) Solubility of fine particles of strontium sulfate. Journal of the American Chemical Society, 82, 4502–4509.

Feenstra, R.M., Stroscio, J.A., Tersoff, J., and Fein, A.P. (1987) Atom-selective imaging of the GaAs(110) surface. Physical Review Letters, 58, 1192–1195.

Frenkel, J. (1930) On the electrical resistance of contacts between solid conductors. Physical Review, 36, 1604–1618.

Golovchenko, J.A. (1986) The tunneling microscope: A new look at the atomic world. Science, 232, 48–53.

Guy, R., Chakrabarti, C., and Schramm, L. (1975) The application of a simple chemical model of natural waters to metal fixation in particulate matter. Canadian Journal of Chemistry, 53, 661–669.

Hansma, P.K., and Tersoff, J. (1987) Scanning tunneling microscopy. Journal of Applied Physics, 61, R1–R23.

Hansma, P.K., Elings, V.B., Marti, O., and Bracker, C.E. (1988) Scanning tunneling microscopy and atomic force microscopy: Application to biology and technology. Science, 242, 209–216.

Hayes, K., and Leckie, J.O. (1986) Mechanism of lead ion adsorption at the goethite-water interface. In J.A. Davis and K.F. Hayes, Eds., Geochemical processes at mineral surfaces, p. 114–141. American Chemical Society, Washington, D.C.

Hayes, K.F., Roe, A.L., Brown, G.E., Jr., Hodgson, K.O., Leckie, J.O., and Parks, G.A. (1987) In situ X-ray absorption study of surface complexes: Selenium oxyanions on $\alpha$-FeOOH. Science, 1987, 783–786.

Hochella, M.F., Jr. (1988) Auger electron and x-ray photoelectron spectroscopies. In F.C. Hawthorne, Ed., Spectroscopic methods in mineralogy and geology. Mineralogical Society of America Reviews in Mineralogy, 18, 573–637.

Hochella, M.F., Jr., and Carim, A.F. (1988) A reassessment of electron escape depths in silicon and thermally grown silicon dioxide thin films. Surface Science, 197, L260–L268.

Hochella, M.F., Jr., Harris, D.W., and Turner, A.M. (1986) Scanning Auger microscopy as a high-resolution microprobe for geologic materials. American Mineralogist, 71, 1247–1257.

Hochella, M.F., Jr., Ponader, H.B., Turner, A.M., and Harris, D.W. (1988a) The complexity of mineral dissolution as viewed by high resolution scanning Auger microscopy: Labradorite under hydrothermal conditions. Geochimica et Cosmochimica Acta, 52, 385-394.

Hochella, M.F., Jr., Lindsay, J.R., Mossotti, V.G., and Eggleston, C.M. (1988b) Sputter depth profiling in mineral-surface analysis. American Mineralogist, 73, 1449–1456.

Holdren, G.R., Jr., and Berner, R.A. (1979) Mechanism of feldspar weathering—I. Experimental studies. Geochimica et Cosmochimica Acta, 43, 1161–1171.

Holdren, G.R., Jr., and Speyer, P.M. (1985) Reaction rate-surface area relationships during the early stages of weathering. I. Initial observations. Geochimica et Cosmochimica Acta, 49, 675–681.

——— (1987) Reaction rate–surface area relationships during the early stages of weathering. II. Data on eight additional feldspars. Geochimica et Cosmochimica Acta, 51, 2311–2318.

Hyland, M.M., and Bancroft, G.M. (1989) An XPS study of gold deposition at low temperature on sulfide minerals: Reducing agents. Geochimica et Cosmochimica Acta, 53, 367–372.

Iler, R.K. (1980) Isolation and characterization of particle nuclei during the polymerization of silicic acid to colloidal silica. Journal of Colloid and Interface Science, 75, 138–148.

Iwasawa, Y., Mason, R., Textor, M., and Somorjai, G.A. (1976) The reactions of carbon monoxide at coordinatively unsaturated sites on a platinum surface. Chemical Physics Letters, 44, 468–470.

Jean, G.E., and Bancroft, G.M. (1985) An XPS and SEM study of gold deposition at low temperatures on sulfide mineral surfaces: Concentration of gold by adsorption/reduction. Geochimica et Cosmochimica Acta, 49, 979–987.

Knauss, K.G., and Wolery, T.J. (1986) Dependence of albite dissolution kinetics on pH and time at 25 °C and 70 °C. Geochimica et Cosmochimica Acta, 50, 2481–2497.

Kurtz, R.L., and Henrich, V.E. (1983) Geometric structure of the $\alpha$-$Fe_2O_3$(001) surface: A LEED and XPS study. Surface Science, 129, 345–354.

Lasaga, A.C., and Blum, A.E. (1986) Surface chemistry, etch pits and mineral-water reactions. Geochimica et Cosmochimica Acta, 50, 2363–2379.

Lawn, B.R., and Wilshaw, T.R. (1975) Fracture of brittle materials, 204 p. Cambridge University Press, Cambridge.

Lee, S.Y., and Jackson, M.L. (1977) Surface charge density determination of micaceous minerals by $^{235}U$ fission particle track method. Clays and Clay Minerals, 25, 295–301.

Loganathan, P., and Burau, R. (1973) Sorption of heavy metal ions by a hydrous manganese oxide. Geochimica et Cosmochimica Acta, 37, 1277–1293.

Michalske, T.A., and Bunker, B.C. (1984) Slow fracture model based on strained silicate structures. Journal of Applied Physics, 56, 2686–2693.

Michalske, T.A., and Freiman, S.W. (1983) A molecular mechanism for stress corrosion in vitreous silica. Journal of the American Ceramic Society, 66, 284–288.

Muir, I.J., Bancroft, G.M., and Nesbitt, H.W. (1989) Characteristics of altered labradorite surfaces by SIMS and XPS. Geochimica et Cosmochimica Acta, 53, 1235–1241.

Onoda, G.Y., and DeBruyn, P.L. (1966) Proton adsorption at the ferric oxide/aqueous solution interface. I. A kinetic study of adsorption. Surface Science, 4, 48–63.

Parfitt, R.L., and Russell, J.D. (1977) Adsorption on hydrous oxides. IV. Mechanisms of adsorption of various ions on goethite. Journal of Soil Science, 28, 297–305.

Parks, G.A. (1984) Surface and interfacial free energies of quartz. Journal of Geophysical Research, 89, 3997–4008.

Perdereau, J., and Rhead, G. (1971) LEED studies of adsorption on vicinal copper surfaces. Surface Science, 24, 555–571.

Petit, J.-C., Della Mea, G., Dran, J.-C., Schott, J., and Berner, R.A. (1987) Mechanism of diopside dissolution from hydrogen depth profiling. Nature, 325, 705–707.

Petrovich, R. (1981) Kinetics of dissolution of mechanically comminuted rock-forming oxides and silicates—II. Deformation and dissolution of oxides and silicates in the laboratory and at the Earth's surface. Geochimica et Cosmochimica Acta, 45, 1675–1686.

Quinn, R.K., Nasby, R.D., and Baughman, R.J. (1976) Photoassisted electrolysis of water using single crystal $\alpha$-$Fe_2O_3$ anodes. Materials Research Bulletin, 11, 1011–1018.

Schneir, J., and Hansma, P.K. (1987) Scanning tunneling microscopy and lithography of solid surfaces covered with nonpolar liquids. Langmuir, 3, 1025–1027.

Schott, J., Brantley, S., Crerar, D., Guy, C., Borcsik, M., and Willaime, C. (1989) Dissolution kinetics of strained calcite. Geochimica et Cosmochimica Acta, 53, 373–382.

Schultz, J., Tsutsumi, K., and Donnet, J.B. (1977a) Surface properties of high-energy solids. I. Determination of the dispersive component of the surface free energy of mica and its energy of adhesion to water and *n*-alkanes. Journal of Colloid and Interface Science, 59, 272–276.

——— (1977b) Surface properties of high-energy solids. II. Determination of the nondispersive component of the surface free energy of mica and its energy of adhesion to water and *n*-alkanes. Journal of Colloid and Interface Science, 59, 277–282.

Seah, M.P., and Dench, W.A. (1979) Quantitative electron spectroscopy of surfaces: A standard data base for electron inelastic mean free paths in solids. Surface and Interface Analysis, 1, 2–11.

Smith, D.P.E., Kirk, M.D., and Quate, C.F. (1987) Molecular images and vibrational spectroscopy of sorbic acid with the scanning tunneling microscope. Journal of Chemical Physics, 86, 6034–6038.

Somorjai, G.A. (1981) Chemistry in two dimensions: Surfaces, 575 p. Cornell University Press, Ithaca, New York.

Tersoff, J., and Hamann, D.R. (1985) Theory of the scanning tunneling microscope. Physical Review B, 31, 805–813.

Tossell, J.A., and Vaughan, D.J. (1987) Electronic structure and the chemical reactivity of the surface of galena. Canadian Mineralogist, 25, 381–392.

Van Hove, M.A., Weinberg, W.H., and Chan, C.-M. (1986) Low-energy electron diffraction: Experiment, theory and surface structure determination, 603 p. Springer-Verlag, New York.

Veblen, D.R., and Buseck, P.R. (1979) Serpentine minerals: Intergrowths and new combination structures. Science, 206, 1398–1400.

Yada, K. (1967) Study of chrysotile asbestos by a high resolution electron microscope. Acta Crystallographica, 23, 704–707.

——— (1971) Study of microstructure of chrysotile asbestos by high resolution electron microscopy. Acta Crystallographica, 27, 659–664.

Zheng, N.J., Wilson, I.H., Knipping, U., Burt, D.M., Krinsley, D.H., and Tsong, I.S.T. (1988) Atomically resolved scanning tunneling microscopy images of dislocations. Physical Review B, 38, 12780–12782.

Manuscript received July 7, 1989
Manuscript accepted August 9, 1989